VALIDATION OF TWO-EQUATION TURBULENCE MODELS FOR HEAT TRANSFER APPLICATIONS

A. Horvat, Y. Sinai

ANSYS CFX, Gemini Building, Fermi Avenue, Harwell Business Centre, Didcot, OX11 0QR
E-mail address of corresponding author: yehuda.sinai@ansys.com

Abstract

The performance of two-equation turbulence models for heat transfer predictions in buoyant flows is investigated. The study compares the k-ε, the RNG k-ε, the SST, and the SSG models. For the k-ε model, a 'scaleable' wall function is used which reduces the sensitivity of the model to the grid near the wall. For the SST model, a near wall model is used, which automatically switches from a low-Reynolds number form to a wall function formulation, based on the grid spacing. Simulations have been carried out for a buoyant plume, a vertical and a horizontal mixed convection jet. The comparison with the experimental correlations of Rouse et al. [9], and Shabbir and George [10] show that the k-ε and the SST model correctly predict velocity and specific weight deficiency distributions, whereas the RNG k-ε and the SSG models are much less dissipative, overpredicting velocity and specific weight deficiency.

I Introduction

Flows arising from thermal buoyancy are frequently encountered in many environmental and man-made systems. In most cases buoyant flows are highly turbulent and often unstable. Moreover, far from the buoyancy source relaminarisation of turbulent flow can also occur. Such complex nature of buoyant flows makes their modelling a very demanding task. As a consequence, for many cases of practical relevance there is still no reliable tool to predict heat or mass transfer coefficients (Hanjalić [1]).

In this paper, the performance of two-equation turbulence models for simulation of buoyancy flows has been investigated. Although, more sophisticated turbulence models (algebraic stress models, large eddy simulation models etc.) are currently available, the two-equations models are still the most used models in industrial applications. The success of the two-equation models is associated with their modest demand for computational resources and robust modelling of flow physics. Nevertheless, they should be applied with caution, especially to cases with buoyancy induced flows.

In the scope of current turbulence models evaluation, the k-ε model (k-ε), the renormalization group k-ε model (RNG k-ε) and the shear stress transport model (SST) have been tested and compared with the more advanced Reynolds stress turbulence model (SSG) developed by Speziale, Sarkar and Gatski [2]. All the models mentioned are available in the standard CFX 5 simulation package. To test the turbulence models, numerical simulations of a vertical buoyant plume, vertical and horizontal mixed convection jets have been performed. The mesh sensitivity analysis has been done for the each case to find a mesh independent solution. The results obtained with different turbulence models have been compared with available experimental data.

II Governing equations of two-equation turbulence models

The basic transport equations used in the CFX 5 package are the continuity equation (1), the momentum equation (2), and the energy equation (3) written here for the Newtonian fluid in the time-averaged form :

$$\partial_t \rho + \partial_j \left(\rho \bar{v}_j \right) = 0 \quad , \tag{1}$$

$$\partial_t \left(\rho \bar{v}_i \right) + \partial_j \left(\rho \bar{v}_j \bar{v}_i \right) = -\partial_i \bar{p} + \partial_j \left(\mu \left(\partial_j \bar{v}_i + \partial_i \bar{v}_j \right) - \frac{2}{3} \mu \left(\partial_l \bar{v}_l \right) \delta_{ji} \right) + g \left(\rho - \rho_{ref} \right) - \partial_j \left(\rho \overline{v_j' v_i'} \right) \quad , \tag{2}$$

$$\partial_t \left(\rho \bar{h} \right) + \partial_j \left(\rho \bar{v}_j \bar{h} \right) = \partial_j \left(\lambda \partial_j \bar{h} \right) - \partial_j \left(\rho \overline{v_j' h'} \right) . \tag{3}$$

This set of transport equations is suitable for simulation of low speed flows (compressible and incompressible) with variable material properties.

Two-equation turbulence models use the gradient diffusion hypothesis to relate the Reynolds stress tensor in the momentum equation (2) to mean velocity gradients:

$$\rho \overline{v_j' v_i'} - \frac{1}{3} \rho \overline{v_k' v_k'} \delta_{ji} = -\mu_t \left(\partial_j \bar{v}_i + \partial_i \bar{v}_j \right) + \frac{2}{3} \mu_t \left(\partial_l \bar{v}_l \right) \delta_{ji} \quad , \tag{4}$$

and the Reynolds flux vector to mean temperature gradient:

$$\rho \overline{v_j' h'} = -\frac{\mu_t}{Pr_t} \partial_j \bar{h} \quad . \tag{5}$$

Therefore, the emphasis is on modelling of eddy diffusivity μ_t. On the contrary, in the algebraic stress models the components of Reynolds stress tensor or the Reynolds flux vector are modelled directly.

II.1 k-ε model

In the k-ε model, the turbulent viscosity μ_t is modelled as

$$\mu_t = C_\mu \rho \frac{k^2}{\varepsilon} \quad , \tag{6}$$

where k is the kinetic energy of turbulent fluctuations and ε is the turbulence dissipation rate:

$$k = \frac{1}{2} \overline{v_l' v_l'} \quad \text{and} \quad \varepsilon = \frac{\mu}{\rho} \overline{\partial_j v_i' \partial_j v_i'} \quad . \tag{7}$$

Two additional transport equations are written for k and ε:

$$\partial_t \left(\rho k \right) + \partial_j \left(\rho \bar{v}_j k \right) = \left(P + G \right) + \partial_j \left(\left(\mu + \frac{\mu}{\sigma_k} \right) \partial_j k \right) - \rho \varepsilon \quad , \tag{8}$$

$$\partial_t \left(\rho \varepsilon \right) + \partial_j \left(\rho \bar{v}_j \varepsilon \right) = C_1 \frac{\varepsilon}{k} P + \partial_j \left(\left(\mu + \frac{\mu}{\sigma_\varepsilon} \right) \partial_j \varepsilon \right) - C_2 \rho \frac{\varepsilon^2}{k} \quad , \tag{9}$$

where P and G are turbulence kinetic energy production terms. Term P represents turbulence production due to shear stress and it is defined as

$$P = \mu_t \left(\partial_j \bar{v}_i + \partial_i \bar{v}_j \right) \partial_j \bar{v}_i - \frac{2}{3} \left(\rho k (\partial_l \bar{v}_l) + 3 \mu_t (\partial_l \bar{v}_l) \partial_j \bar{v}_i \right) \delta_{ji} . \tag{10}$$

The term G describes generation of turbulence due to volumetric forces; in our case, this is due to buoyancy:

$$G = -\frac{\mu_t}{\rho Pr_t}\left(g_j \partial_j \rho\right).$$

(11)

In the standard k-ε model, C_μ, C_1, C_2, σ_k, σ_ε and Pr_t are empirically determined coefficients. Their values are constant and listed in Table 1.

Table 1: The standard k-ε model coefficients.

C_μ	C_1	C_2	σ_k	σ_ε	Pr_t
0.09	1.44	1.92	1.0	1.3	0.9

II.2 Renormalization group k-ε model

The renormalization group k-e model was initially proposed by Yakhot et al. [3]. It is based on the Renormalization Group Theory (RNG) applied to fluid flow transport equations. The form of transport equations for turbulence kinetic energy k and turbulence dissipation rate ε is the same as in the standard k-ε:

$$\partial_t(\rho k) + \partial_j\left(\rho \bar{v}_j k\right) = P + \partial_j\left((\mu + \frac{\mu}{\sigma_k})\partial_j k\right) - \rho\varepsilon,$$

(12)

$$\partial_t(\rho\varepsilon) + \partial_j\left(\rho \bar{v}_j \varepsilon\right) = \left(C_1 - C_{1,RNG}\right)\frac{\varepsilon}{k}P + \partial_j\left((\mu + \frac{\mu}{\sigma_\varepsilon})\partial_j \varepsilon\right) - C_2\,\rho\frac{\varepsilon^2}{k},$$

(13)

but the role and values of the model's coefficients are modified. The coefficient $C_{1,RNG}$ is modelled further as

$$C_{1,RNG} = \frac{\eta(1 - \eta/\eta_0)}{1 + \beta\eta^3}$$

(14)

where η represents the non-dimensional strain rate defined as

$$\eta = \sqrt{\frac{P}{\rho C_{\mu,RNG}\varepsilon}}\ .$$

(15)

The other coefficients $C_{\mu,RNG}$, C_1, C_2, C_3, σ_k, σ_ε, η_0, β and Pr_t are constant and listed in Table 2.

Table 2: The renormalization group k-ε model coefficients.

$C_{\mu,RNG}$	C_1	C_2	σ_k	σ_ε	η_0	β	Pr_t
0.085	1.42	1.68	1.0	1.3	4.38	0.012	0.9

II.3 Shear stress transport model

The shear stress transport model (SST) was developed and improved by Menter [4 & 5]. It is a combination of the k-ε and the k-ω model of Wilcox [6], where the turbulence eddy frequency

$$\omega = \frac{\rho k}{\mu_t} \tag{16}$$

is used instead of turbulence dissipation rate ε. The idea behind the SST model is to combine the best elements of the k-ε and the k-ω model with the help of a blending function F_1:

$$F_1 = tanh\left(arg_1^4\right) \tag{17}$$

where $arg_1 = min\left(max\left(\dfrac{\sqrt{k}}{\beta^* \omega y}; \dfrac{500\mu}{\rho \omega y^2} \right); \dfrac{4\sigma_{\omega 2} \rho k}{CD_{k\omega} y^2} \right)$ and $CD_{k\omega} = max\left(\dfrac{2\sigma_{\omega 2} \rho \partial_j k \partial_j \omega}{\omega}; 10^{-10} \right)$.

The blending function F_1 is one at the wall and zero far away from the wall, thus activating the Wilcox model in the near-wall region and the k-ε model for the rest of the flow:

$$\text{SST model} = F_1 \cdot (k\text{-}\omega \text{ model}) + (1\text{-}F_1) \cdot (k\text{-}\varepsilon \text{ model}) . \tag{18}$$

To combine the k-ε and the k-ω model, the transport equations of both models have to be written in the same form. Therefore, the k-ε model transport equations (8 & 9) have been transformed into k and ω transport equations. Using scheme (18), the transport equation for turbulence kinetic energy k has been formulated as

$$\partial_t(\rho k) + \partial_j\left(\rho \bar{v}_j k\right) = P + \partial_j\left((\mu + \frac{\mu}{\sigma_{k3}})\partial_j k \right) - \beta^* \rho \omega k , \tag{19}$$

and for turbulence eddy frequency ω as

$$\partial_t(\rho \omega) + \partial_j\left(\rho \bar{v}_j \omega\right) = \alpha_3 \frac{\omega}{k} P + \partial_j\left((\mu + \frac{\mu}{\sigma_{\omega 3}})\partial_j \omega \right) + (1 - F_1)\frac{2\rho}{\sigma_{\omega 2}} \partial_j k \partial_j \omega - \beta_3 \rho \omega^2 . \tag{20}$$

With this approach, the attractive near-wall performance of the Wilcox model has been utilised without the potential errors resulting from the free stream sensitivity of that model.

Based on turbulence kinetic energy k and turbulence eddy frequency ω, eddy viscosity μ_t has been defined as

$$\mu_t = \rho \frac{a_1 k}{max(a_1 \omega; SF_2)} , \tag{21}$$

where S is an invariant measure of the strain rate, $F_2 = tanh\left(arg_2^2\right)$ and $arg_2 = max\left(\dfrac{2\sqrt{k}}{\beta^* \omega y}; \dfrac{500\mu}{\rho \omega y^2} \right)$.

The values of the coefficients β^*, $\sigma_{\omega 2}$, σ_{k3}, α_3, $\sigma_{\omega 3}$, β_3, a_1 and Pr_t , which are used in the SST model, are in Table 3. Note that the coefficients σ_{k3}, α_3, $\sigma_{\omega 3}$ and β_3 are not constant. These coefficients' values are calculated locally during a simulation from the values of the k-ω and the k-ε model using scheme (18).

Table 3: The shear stress transport model coefficients.

β^*	$\sigma_{\omega 2}$	σ_{k3}	α_3	$\sigma_{\omega 3}$	β_3	a_1	Pr_t
0.09	1.168	2.0-1.0	5/9-0.44	2.0-1.168	0.075-0.0828	0.31	0.9

III Test cases

Three different cases of buoyant air flow have been studied by numerical simulations with the k-ε, the RNG k-ε, the SST and the SSG turbulence. In all cases the air ambient temperature has been taken as $T_{amb} = 25\ ^o\text{C}$.

The major parameter governing the flow above the small axisymmetric source of buoyancy is specific buoyancy flux (Turner [8]) defined as

$$F_0 = 2\pi\int_0^R wb\,rdr \ , \tag{22}$$

where $b = g(\rho_{amb} - \rho)/\rho_{amb}$ is the specific weight deficiency. The specific buoyancy flux F_0 is preserved throughout the flow and depends only on source conditions. When momentum is also introduced at the source, conservation of specific momentum flux M_0 becomes important. As turbulence isotropy is being assumed in the two-equation model, specific momentum flux M_0 may defined as

$$M_0 = 2\pi\int_0^R w^2\,rdr \ . \tag{23}$$

The simulation results have been carefully analysed. As most of experimental data exist for the self-similar region of free-shear flows (List [11]), the vertical velocity w has been scaled as

$$w = F_0^{1/3}z^{-1/3}f\left(r\right) \ , \tag{24}$$

and the specific weight deficiency b as

$$b = F_0^{2/3}z^{-5/3}f\left(r\right) \ . \tag{25}$$

The function $f(r)$ represents plume's radial behaviour and acquire a constant form in the self-similar region $z > 60R$.

In the presented work, the calculated centreline distributions of vertical velocity and specific weight deficiency have been compared with the experimental findings of Rouse et al. [9]:

$$w_c = 4.6F_0^{1/3}z^{-1/3} \ , \tag{26}$$

$$b_c = 11.0F_0^{2/3}z^{-5/3} \ , \tag{27}$$

and Shabbir and George [10] :

$$w_c = 3.4F_0^{1/3}z^{-1/3}, \tag{28}$$

$$b_c = 9.4F_0^{2/3}z^{-5/3}. \tag{29}$$

They performed comprehensive experimental measurements of buoyant plumes and vertical mixed convection jets.

III.1 Vertical buoyant plume

In the case of a vertical buoyant plume, the simulation domain is a 30° slice of a cylinder (Fig.1). Buoyancy as a source of air motion arises from volumetric heating in a part of the simulation domain that is coloured red in Fig 1. Its radius is $R = 2.5$ cm.
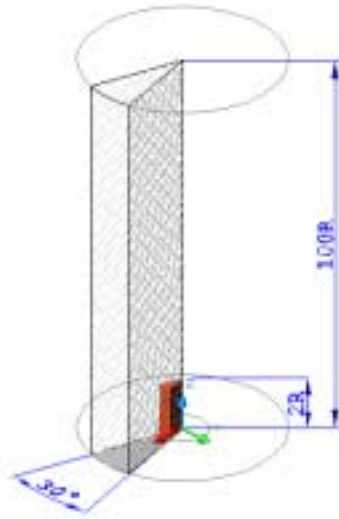

Figure 1: Simulation domain for the vertical buoyant plume

Two sets of simulations have been performed. In the first set the volumetric heating rate has been $I_g = 0.6057$ W/cm^3 for which the Grashof number is 10^8. Due to the modest temperature increase $T\text{-}T_{amb}$, the Boussinesq approximation of buoyant force (ρ_{amb} - ρ) ~ ρ_{amb} β ($T\text{-}T_{amb}$) has been used. The second set of simulations has been performed for volumetric heating $I_g = 6.057$ W/cm^3. The resulting Grashof number is 10^{10} and the temperature difference $T\text{-}T_{amb}$ is much higher than in the first set. Therefore, the full compressible flow model has been used in the second set.

Both sets of simulations have been performed with the k-ε, the RNG k-ε, the SST and the SSG turbulence model. Based on the recommendations of Nam and Bill [7] for buoyant flows, some of the standard k-ε model coefficients have been modified. The values of C_μ and Pr_t have been changed to 0.18 and 0.85, respectively.
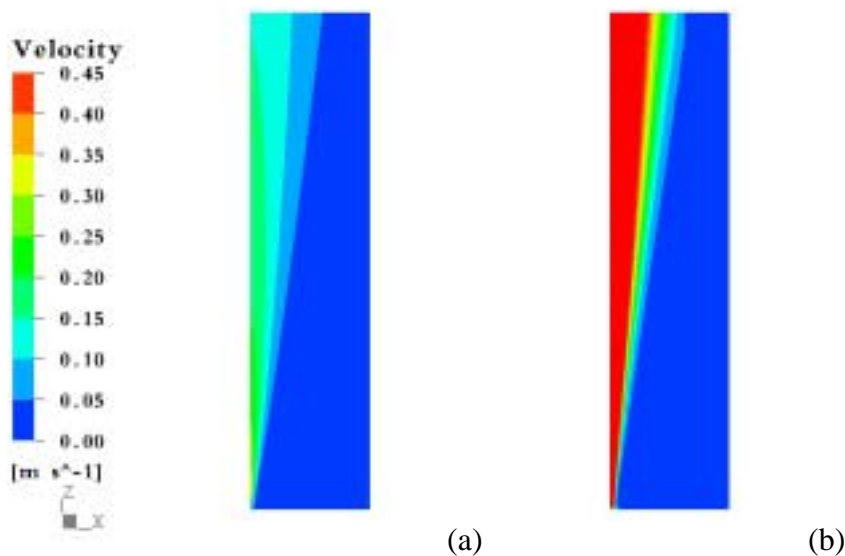

Figure 2: Velocity field of the buoyant plume, k-ε (N & B) model; (a) $Gr = 10^8$, (b) $Gr = 10^{10}$

Figures 2 and 3 present velocity and temperature fields obtained with the modified k-ε model of Nam and Bill [7] for Grashof numbers $Gr=10^8$ (a) and $Gr=10^{10}$ (b).
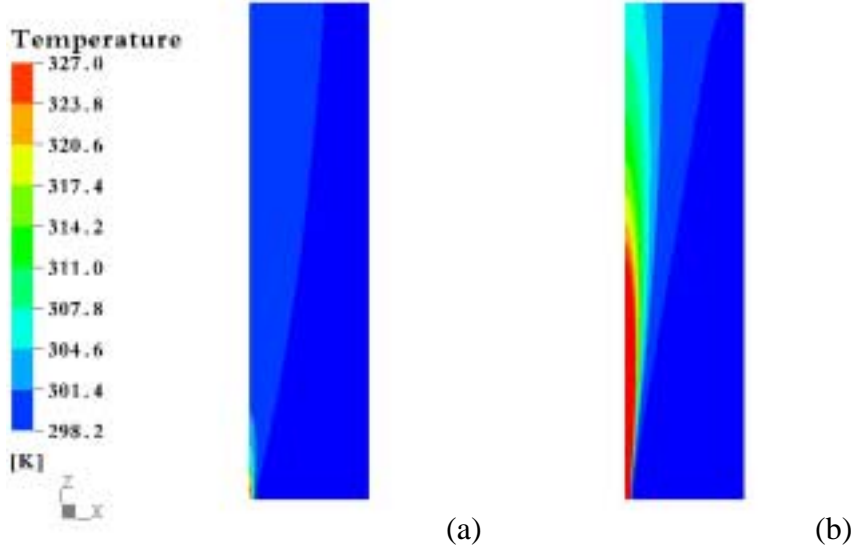

(a)   (b)

Figure 3: Temperature field of the buoyant plume, k-ε (N & B) model; (a) $Gr=10^8$, (b) $Gr=10^{10}$

In general, when temperature differences are not too large, the Boussinesq simplification may be used to approximate specific weight deficiency b. Introducing an additional expression for energy balance $c_p \rho_{amb} w(T - T_{amb})A_\perp \sim I_g V_g$, the specific buoyancy flux (22) can be written as

$$F_0 = \frac{g \beta I_g V_g}{c_p \rho_{amb}} \quad . \tag{30}$$

Figure 4 presents a comparison of the vertical velocity along the plume's centreline w_c for Grashof numbers $Gr=10^8$ (a) and $Gr=10^{10}$ (b). The results have been obtained with different turbulence models and compared with the experimental correlations (26 & 28).

(a)   (b)
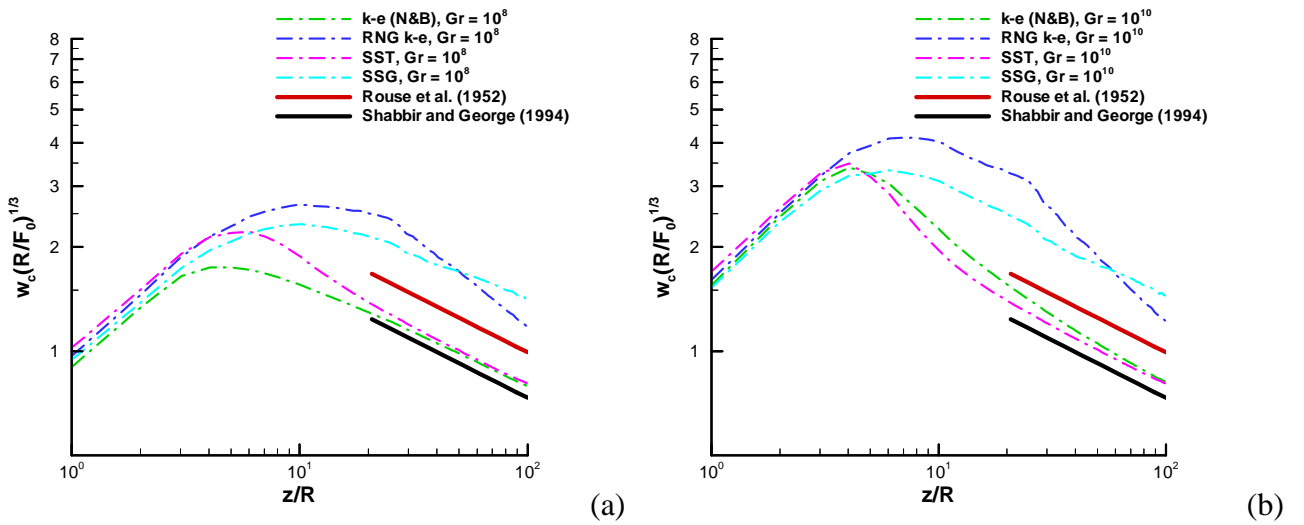
Figure 4: Vertical velocity along the centreline w_c ; (a) $Gr=10^8$, (b) $Gr=10^{10}$

The calculated specific weight deficiency along the plume's centreline b for Grashof numbers $Gr = 10^8$ (a) and $Gr = 10^{10}$ (b) is presented in Fig 5. The results have been compared with the experimental correlations (27 & 29).
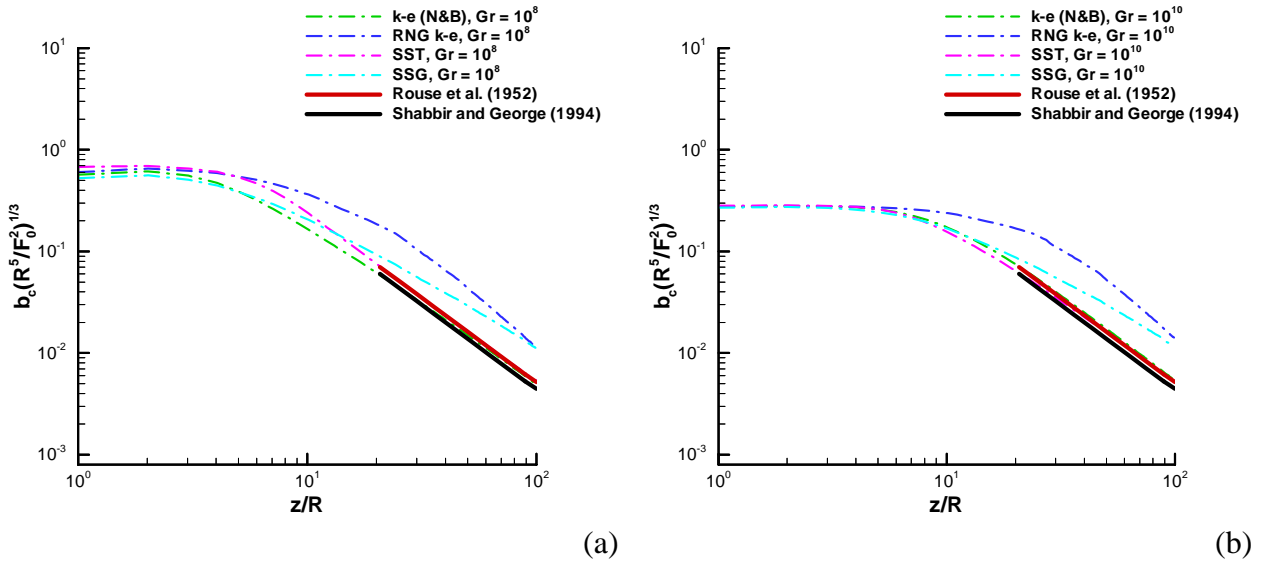

(a)   (b)

Figure 5: Spec. weight deficiency along the centreline b_c ; (a) $Gr = 10^8$, (b) $Gr = 10^{10}$

III.2 Vertical mixed convection jet

The simulation domain has been a 30° slice of a cylinder with an inlet pipe (Fig.2). Heated turbulent flow has been introduced through the inlet pipe with a radius $R = 2.5$ cm into ambient.
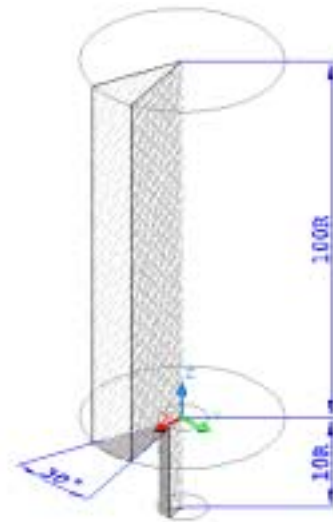
Figure 6: Simulation domain for the vertical mixed convection jet

In order to realistically simulate the development of the jet, a separate simulation of flow in the inlet pipe has been performed to obtain radial profiles of velocity w, turbulence kinetic energy field k and turbulence dissipation rate ε. These profiles have been than used as the inlet boundary conditions.

A set of simulations have been performed for Richardson number $Ri = 1.0$ with Reynolds number $Re = 4078$ and Grashof number $Gr = 16.63 \cdot 10^6$. As the inflow temperature has been set to

T_{inlet} = 950 ^oC, the full compressible flow model has been applied in all simulations. Each simulation has been performed with the k-ε (N & B), the RNG k-ε, the SST or the SSG turbulence model and the results have been compared with the correlations obtained from the experimental data of Rouse et al, [8], and Shabbir and George [9].

Figures 7 and 8 present velocity and temperature fields obtained with the k-ε (N & B) turbulence model for Richardson number Ri =1.0 (Re = 4078 and Gr =16.63·10^6).
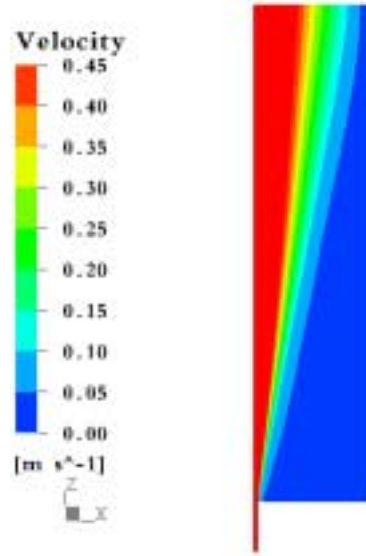
Figure 7: Velocity field of the vertical mixed convection jet, k-ε (N & B) model; Ri=1.0, Re=4078, Gr=16.63·10^6
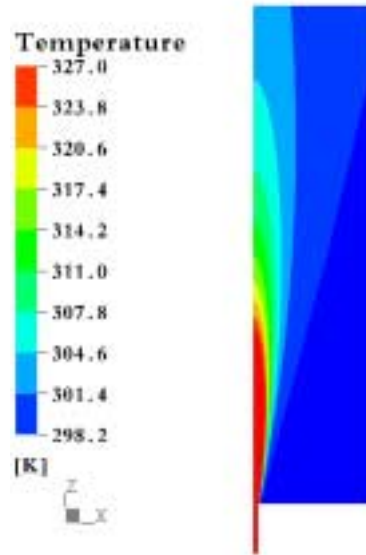

Figure 8: Temperature field of the vertical mixed convection jet, k-ε (N & B) model; Ri=1.0, Re=4078, Gr=16.63·10^6

In the mixed convection jet, the flow close to the source behaves like a buoyant jet. As the flow evolves, buoyancy overwhelms the momentum that is introduced through the inflow. After a certain distance characterised by the Morton's lengthscale [9]

$$L_M = \frac{M_0^{3/4}}{F_0^{1/2}} \, , \tag{31}$$

9

the flow is governed by buoyancy alone. Figure 9 presents comparison of the vertical velocity along the plume's centreline w_c for Richardson number Ri=1.0.
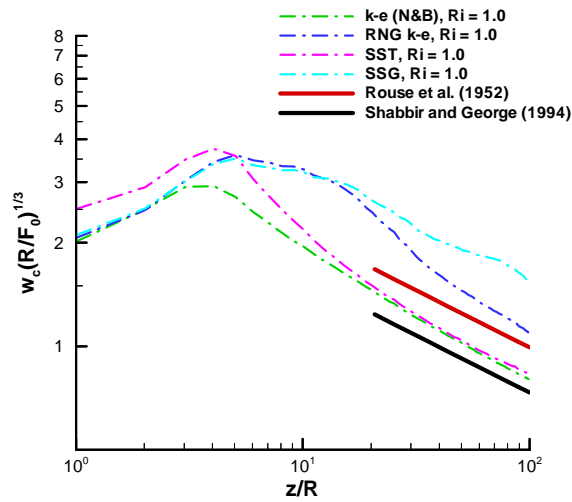

Figure 9: Vertical velocity along the centreline w_c ; Ri=1.0

The calculated specific weight deficiency along the plume's centreline for Richardson number Ri=1.0 is presented in Fig 10.
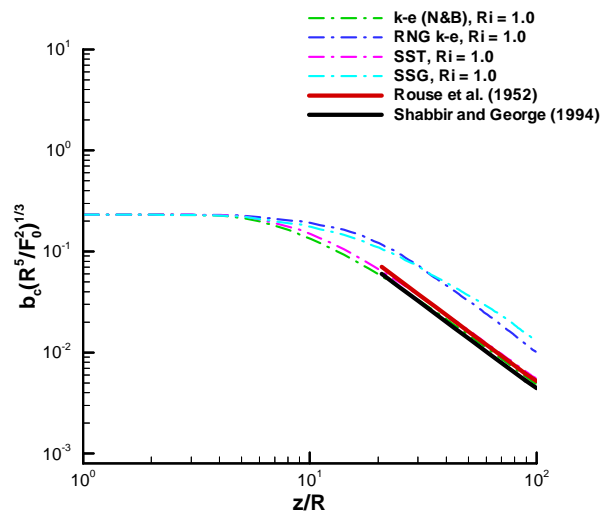

Figure 10:   Spec. weight deficiency along the centreline b_c ; Ri=1.0

III.3 Horizontal mixed convection jet

In this case, heated air is horizontally introduced into ambient through an inlet pipe (Fig.11) with a radius $R = 2.5$ cm. As the problem is symmetrical, the simulation domain occupies only 1/2 of the flow field.
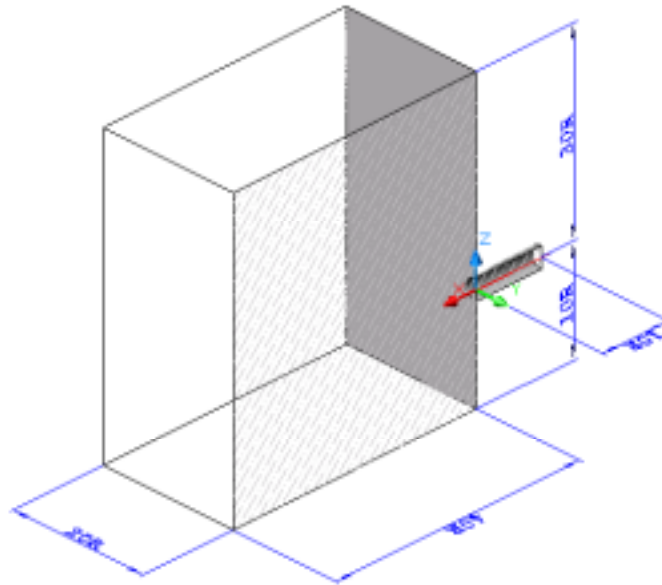
Figure 11: Simulation domain for the horizontal mixed convection jet

Two sets of simulations have been performed for two different Richardson numbers. In both sets, the full compressible flow model has been used. The first set of calculations has been performed for Richardson number $Ri=0.1$, with Reynolds number $Re = 4078$ and Grashof number $Gr =1.58 \cdot 10^6$. The temperature of the inflow has been set to $T_{inflow} = 113$ ^{o}C. The radial profiles of velocity u, turbulence kinetic energy k and turbulence dissipation rate ε in the inlet pipe have been separately calculated to realistically assess the inflow conditions. The second set of calculations has been done for Richardson number $Ri=10$, with Reynolds number $Re = 1290$ and Grashof number $Gr =16.63 \cdot 10^6$. The inlet temperature has been set to $T_{inflow} = 950$ ^{o}C. As the Reynolds number is small in the second set, a parabolic velocity profile has been prescribed at the inlet. Both sets of simulations have been performed with the k-ε (N & B), the RNG k-ε, the SST and the SSG turbulence model.

Figures 12 and 13 present velocity and temperature fields obtained for Richardson numbers $Ri=0.1$ and $Ri=10$. In later case, the wall influence becomes important therefore the SST model should be most appropriate to capture the wall boundary layer.
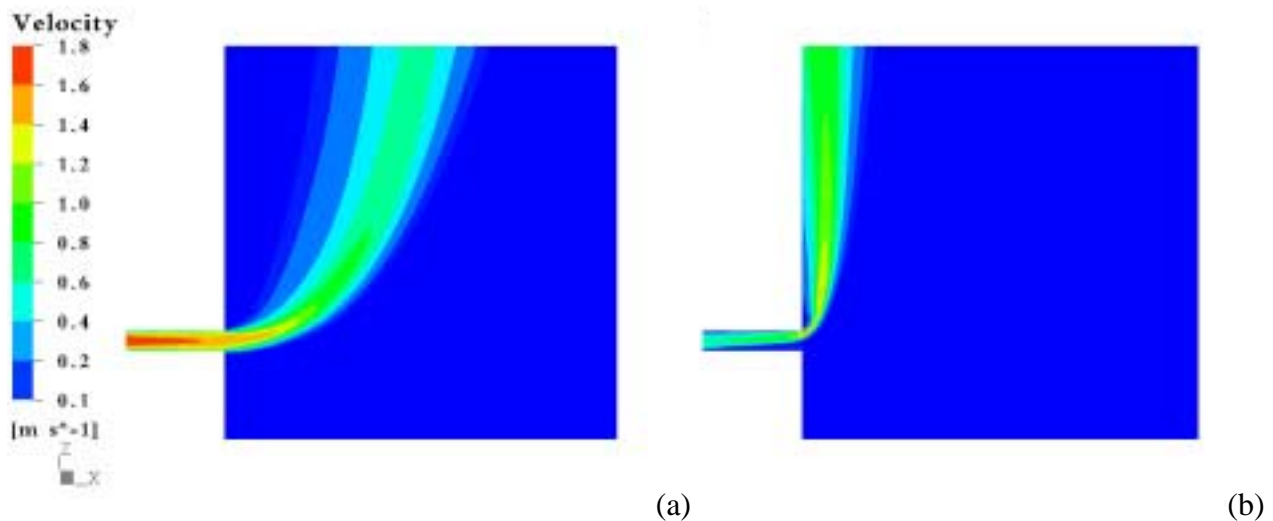

(a)   (b)

Figure 12:   Velocity field of the horizontal mixed convection jet;
(a) k-ε (N & B) model; $Ri = 0.1$, $Re=4078$, $Gr =1.58 \cdot 10^6$,
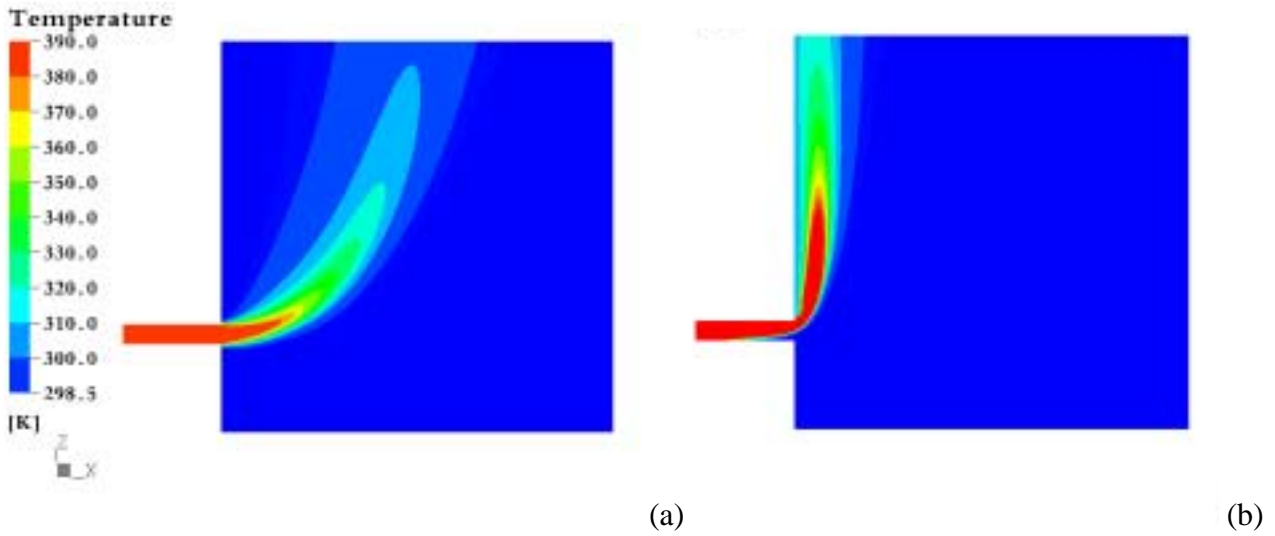(b) SST model; $Ri = 10$, $Re=1290$, $Gr =16.63 \cdot 10^6$

11

Figure 13: Temperature field of the horizontal mixed convection jet;
(a) k-ε (N & B) model; $Ri = 0.1$, $Re = 4078$, $Gr = 1.58 \cdot 10^6$,
(b) SST model; $Ri = 10$, $Re = 1290$, $Gr = 16.63 \cdot 10^6$

     The horizontal mixed convection jet is governed by the competing specific momentum flux (23) in the horizontal direction and the specific buoyancy flux (22) in the vertical direction. Maximum vertical velocity w_{max} and specific weight deficiency b_{max} at the symmetry plane have been scaled the same way as the centreline velocity w_c and specific weight deficiency b_c in the case of the buoyant plume and the vertical mixed convection jet (24 & 25). Since we have been unable to find suitable experimental results for this specific case, the comparison with the correlations of Rouse [9], and Shabbir and George [10] will help us to explain some additional effects. Figures 14 presents comparison of the maximum vertical velocity w_{max} at the symmetry plane for Richardson number $Ri = 1.0$ (a) and for Richardson number $Ri = 10$ (b).
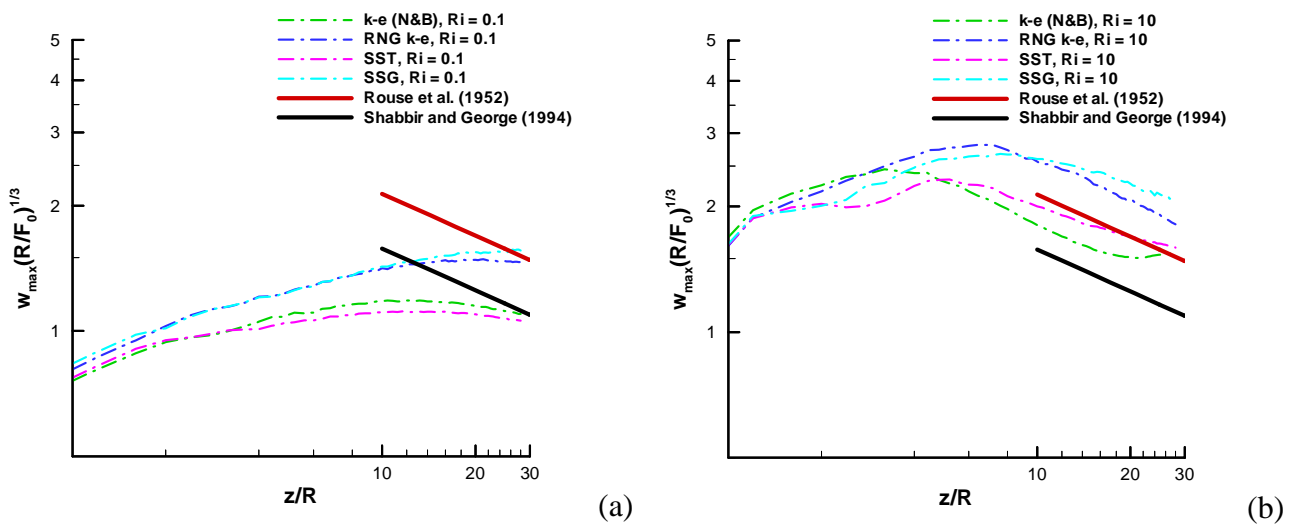

Figure 14: Max. vertical velocity at the symmetry plane w_{max}; (a) $Ri = 0.1$, (b) $Ri = 10$

The maximum specific weight deficiency at the symmetry plane for Richardson numbers $Ri = 0.1$ and $Ri = 10$, is presented in Fig 15.
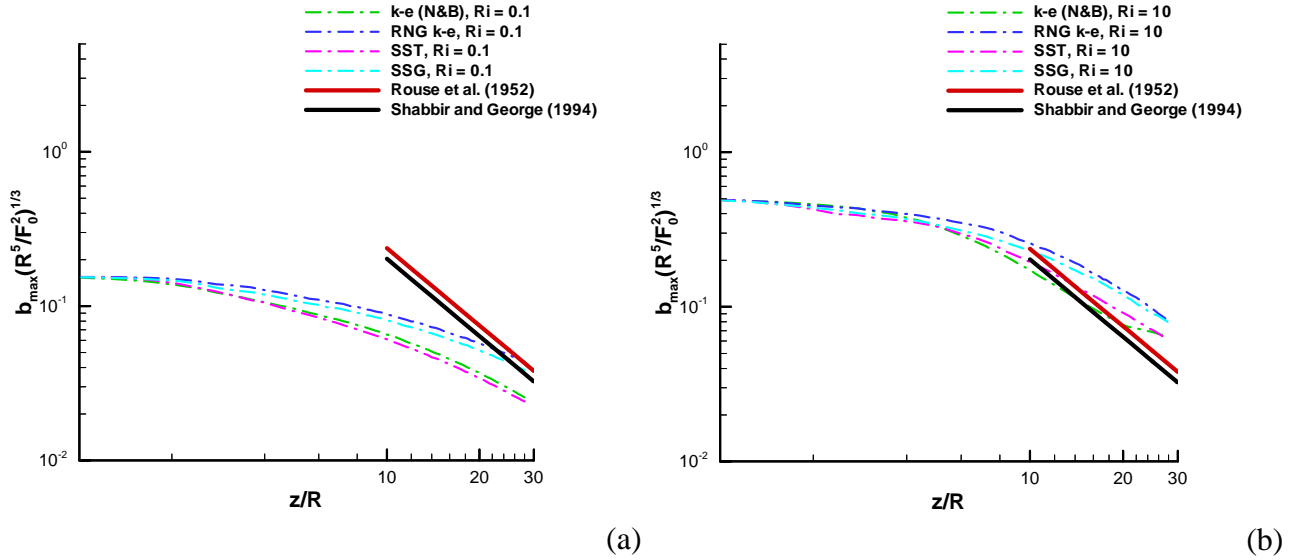
Figure 15: Max. specific weight deficiency at the symmetry plane b_{max}; (a) Ri=0.1, (b) $Ri = 10$

VI Discussion

For the investigated cases of free-shear flows, all the tested turbulence model correctly predict trends of velocity and temperature distribution. Nevertheless, there are significant differences.

Analysing the vertical centreline velocity w_c in the plume (Fig. 4), it can be observed that all the tested turbulence models produce same results in the first region of the developing plume ($z/R < 4$). In this region, the dominant mechanisms are buoyancy that accelerates the plume and shear stresses between the buoyant core and the surrounding fluid that generate turbulence production. The differences between the turbulence models become larger in the intermediate region ($8 < z/R < 40$) where flow changes its nature. Here, the RNG k-ε and the SSG model overpredict the centreline velocity w_c. In the self-similar region ($40 < z/R$), where the plume slowly decays, only the RNG k-ε model fails to predict the trend of decreasing velocity $w_c \sim z^{-1/3}$. The same conclusion can be drawn for the centreline distribution of specific weight deficiency b_c in Fig. 5.

In the case of the vertical mixed convection jet, the first region ($z/R < 4$) is strongly under the influence of the introduced momentum flux M_0. The fluid velocity is higher than in the case of buoyant plume, with less evident flow acceleration. After the distance of the Morton's lengthscale ($L_M \sim 4R$), buoyancy plays the dominant role. In the intermediate region ($4 < z/R < 40$), the velocity starts to decrease. The results of the RNG k-ε and the SSG model show identical values that are much higher than the results of the k-ε (N & B) and the SST model. Unfortunately, we were unable to find any experimental data covering the intermediate region that can be used for comparison. In the self-similar region ($40 < z/R$), the velocities calculated with the k-ε (N & B) and the SST model are much closer to the experimental correlations (26 & 28) than the RNG k-ε and the SSG model results. There is much less difference between distributions of specific weight deficiency along the centreline b_c. Nevertheless, the k-ε (N & B) and the SST model results are again closer to the experimental correlations (27 & 29).

For the case of the horizontal mixed convection jet, no appropriate experimental data were found. Therefore, it is hard to deduce which turbulence model performs better. At low Richardson number $Ri = 0.1$, the buoyant jet slowly changes its orientation from horizontal to vertical direction due to weak buoyancy force (Figs. 12a and 13a). When the Richardson number is increased to Ri=10, the buoyancy force bends the jet into vertical direction immediately after leaving the inlet pipe (Figs. 12b and 13b). This causes interaction between the jet and the wall as previous reported

by Jaluria [12]. The velocity distributions w_{max} obtained with the k-ε (N & B) and the SST model (Fig. 14b) show a rapid acceleration where the core of the plume touches the wall. Due to stronger buoyancy in the high Richardson number case (Fig. 14b and 15b), the distributions of maximum vertical velocity w_{max} and specific weight deficiency b_{max} approach to the experimental correlations faster than in the low Richardson number case (Fig. 14a and 15a). As already observed previously, the RNG k-ε and the SSG turbulence model are much less dissipative, which results in higher values of calculated velocity w_{max} and specific weight deficiency b_{max}.

Nomenclature

Latin letters

$A_\perp$	ground area of V_g	P	production of k due to shear stress
b	specific weight deficiency	Pr	Prandtl number
c_p	specific heat	r	radial coordinate
F_0	specific buoyancy flux	R	radius
F_1, F_2	SST model blending functions	Ri	Richardson number
g	gravitational acceleration	S	invariant measure of the strain rate
G	production of k due to buoyancy	T	temperature
Gr	Grashof number	u	horizontal velocity
h	specific enthalpy	v	velocity
I	volumetric heating rate	V_g	heated volume
k	turbulence kinetic energy	w	vertical velocity
L_M	Morton's lengthscale	x	horizontal coordinate
M_0	specific momentum flux	z	vertical coordinate
p	pressure		

Greek letters | | Subscripts/Superscripts

β	thermal expansion coefficient	amb	ambient value
ε	turbulence dissipation rate	c	centreline
ρ	density	max	maximum value at the symmetry plane
η	represents non-dimensional strain rate	ref	reference value
λ	thermal conductivity	t	turbulence variable
μ	dynamic viscosity		Symbols
ω	turbulence eddy frequency	$'$	fluctuation
		$^-$	time-averaging (incompressible model), Favre-averaging (compressible model)

References

[1] K. Hanjalić, Achievements and Limitations in Modelling and Computation of Buoyant Turbulent Flows and Heat Transfer, *10th Int. Heat Transfer Conf.*, Vol. 1, Brighton, UK, Proceedings, pp.1-18, 1994.

[2] C. G. Speziale, S. Sarkar, T. B. Gatski, Modelling the Pressure-Strain Correlation of Turbulence: An Invariant Dynamical Systems Approach, *J. Fluid Mechanics*, Vol. 277, pp. 245-272, 1991.

[3]   V. Yakhot, S.A. Orszag, Renormalization Group Analysis of Turbulence. I. Basic Theory, *J. Sci. Computing*, 1, 3, pp. 245-272, 1986.

[4]   F. R. Menter, Multiscale Model for Turbulent Flows, *24th Fluid Dynamics Conference. American Institute of Aeronautics and Astronautics*, Proceedings, p. 38, 1993.

[5]   F. R. Menter, Two-Equation Eddy-Viscosity Turbulence Models for Engineering Applications, *AIAA-Journal*, Vol. 32, No. 8, pp. 37- 40, 1994.

[6]   D. C. Wilcox, Multiscale Model for Turbulent Flows, *AIAA 24th Aerospace Sciences Meeting*, American Institute of Aeronautics and Astronautics, Proceedings, p. 37, 1986.

[7]   S. Nam, R. G. Bill Jr., Numerical Simulation of Thermal Plumes, *Fire Safety J.*, 21, pp. 231-256, 1993.

[8]   J. S. Turner, *Buoyancy Effects in Fluids: Buoyant Convection from Isolated Sources*, Cambridge University Press, Cambridge, UK, pp. 165-206, 1973.

[9]   H. Rouse, C. S. Yih, H. W. Humphreys, Gravitational Convection from a Boundary Source, *Tellus*, 4, pp. 201-210, 1952.

[10]   A. Shabbir, W. K. George, Experiments on a Round Turbulent Buoyant Plume, *J. Fluid Mech.*, Vol. 275, pp. 1-32, 1994.

[11]   E. J., List, *Turbulent Buoyant Jets and Plumes: Mechanics of Turbulent Buoyant Jets and Plumes*, Ed. Rodi, W., Pergamon Press, Oxford, UK, 1982.

[12]   Y. Jaluria, *Natural Convection*, Eds. Kakac, S., Aung, W., Viskanta, R., Francis and Taylor, Washington D.C., pp. 51-74, 1985.